DOI: 10.3217/978-3-99161-057-1-152

Detailed material testing of adobe structures to complete a comprehensive SHM approach that includes laser scanning and ambient vibration studies

Shakhzod Takhirov[1,0000-0002-4396-7946], Zukhritdin Ergashev[2,0000-0002-9280-0616], Bakhodir Rakhmonov[3,0000-0001-6285-2063], Amir Gilani[4], Mirzokhid Akhmedov[5], Ravshan Shamansurov[6]
[1]University of California - Berkeley, Berkeley, California, United States of America;
[2]Tashkent State Transport University, Tashkent, Uzbekistan;
[3]Urgench State University, Urgench, Uzbekistan;
[4]Miyamoto International, Sacramento, California, United States of America;
[5]Miyamoto International - Silk Road, Tashkent, Uzbekistan;
[6]Sigma Innovative Tech, Tashkent, Uzbekistan
email: takhirov@berkeley.edu, ergashev33@gmail.com, Rah-Bahodir@yandex.ru, agilani@miyamotointernational.com, m.akhmedov@miyamotointernational.com, shamansurov@rambler.ru.

ABSTRACT: The research team, comprising international and local experts, has been studying heritage adobe buildings in Uzbekistan for several years. A few field studies were conducted at the heritage sites of Uzbekistan and Karakalpakstan: Toprak-Kala, Chadra Hauli, Ulli Hovli, and many others. As the first step of the comprehensive research strategy, laser scanning was used to generate accurate digital twins of the heritage structures. A non-destructive ambient vibration study of selected structures was conducted in the second step. This in-situ testing measures resonant frequencies and mechanical properties at very small excitations, which is insufficient for accurate numerical modeling. This study was conducted to address this shortcoming. A few adobe structures constructed of pakhsa were selected. Since the pakhsa is made of clay, which is available in the vicinity of the construction site, the exact georeferencing of each structure was considered. A few cylindrical samples were bored out from the walls of the structures and tested at the University of California, Berkeley. The samples were instrumented with strain gages, and they were investigated in compression and split tests. As a result of this study, Young's modulus, Poisson's ratio, and the strength of each test specimen were measured. These parameters will be used to generate more accurate numerical models of the structures and assess the advantages of reinforcement strategies for heritage structures.

KEY WORDS: Adobe heritage structures; structural health monitoring; pakhsa; numerical modeling; laser scanning.

1 GENERAL GUIDELINES

Buildings made of adobe materials are very common throughout the world. They represent a very affordable way of construction, utilizing local materials. In addition, the adobe buildings are environmentally friendly because their construction uses natural, renewable materials and energy-efficient construction methods. As a result, this construction has a smaller carbon footprint compared to conventional construction. In addition, the adobe buildings naturally retain heat inside longer during winter and preserve a cooler room environment on hot summer days.

The adobe construction is very common in Central Asian countries and is considered one of the traditional construction techniques in these regions. Adobe buildings can last a very long time. For example, the adobe structures of Toprak-Kala (Uzbekistan) are dated to the 2nd and 3rd centuries CE (Common Era). They still have an adequate structural health condition, as evaluated in a laser scanning study [1]. A recent discovery of previously unknown ancient cities, Tashbulak and Tugunbulak (Uzbekistan), revealed that these cities have adobe buildings dated to the 6th –11th century CE [2]. Another recent example is the four-story-tall Chadra Hauli in Uzbekistan, constructed in 1871 and still in excellent structural shape, as studied by using a laser scanner [3]. More than 200 Adobe buildings of more recent construction have been studied in rural areas of Tajikistan [4]. All of these structures are good representatives of pakhsa construction.

2 COMPREHENSIVE SHM APPROACH AND OBJECTIVES OF THIS PAPER

2.1 SHM of adobe buildings with performance prediction

A comprehensive approach is undertaken for the structural evaluation of the heritage structures and the prediction of their performance under various loading conditions. The structural evaluation and assessment are conducted using laser scanning technology to capture the current condition of heritage monuments in 3D accurately, as shown in Figure 1.

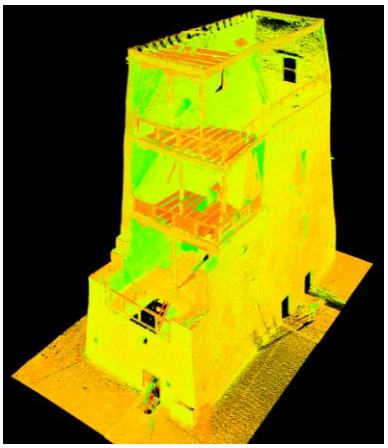

Figure 1. 3D point cloud of a heritage building collected by a laser scanner [3].

DOI: 10.3217/978-3-99161-057-1-152

Based on the analysis of the point clouds collected by the laser scanner, all anomalies of the monuments are identified and studied in detail. Based on the 3D geometry captured by the laser scanner, an accurate finite element is created to investigate its structural performance under various loading conditions, as presented in Figure 2.

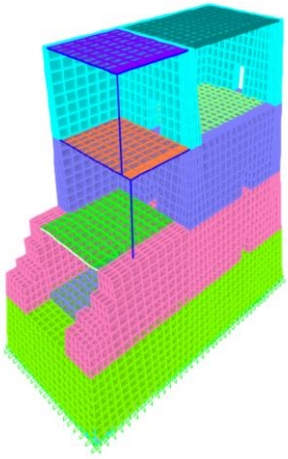

Figure 2. A finite element model of a heritage building was generated from the point cloud.

The finite element model requires input of the material properties of adobe to generate a realistic model. This information is difficult to obtain, as it relates to destructive testing, which is not permitted for heritage structures. Even if the collection of the sample is permitted, the benefits of the sample testing need to be investigated to optimize the sample set and the sample collection methods. This paper focuses on the development of a sample collecting procedure, a procedure for the preparation of collected samples for testing, and a procedure for testing to measure major material properties of the samples. These procedures are developed by investigating two buildings constructed of the same material as the heritage building, pakhsa. It is worth noting that there are a few standards focused on testing adobe samples, see [9], as a representative example. Still, their scope is very limited and does not provide any adequate guidance on reliable procedures for measuring the Young's modulus and Poisson's ratio.

2.2 Material properties of adobe: A brief review of the previous work

Adobe represents a man-made construction material that utilizes the raw earth material usually available close to the construction site. Hence, its mechanical characteristics depend on many parameters. These parameters can be as follows: the quality of earth material available for construction, the curing time of the clay before forming it into a wall or a brick, the way the clay was placed into the walls, bonding aggregates added to the earth material (if any), the quality of the craftsmanship work, the curing process after forming the wall, and many others. After the completion of construction, the mechanical properties can be affected by moisture. Therefore, there is substantial variability in the mechanical properties of adobe materials used in or taken from structures worldwide [5]. The mechanical properties are estimated by testing samples taken from adobe walls or created during construction (which is very rare). The samples can be collected in the form of cubes, prisms, and cylinders, and the test results also depend on the shape of the test specimen [6]. For example, based on a comparative analysis of test results for cylinders [7] and [8], the Young's modulus of the adobe material varies by a factor of ten.

3 TESTING ADOBE CYLINDERS

3.1 General description of samples

The samples were collected from existing buildings at specific locations away from structurally critical areas. Two buildings were included in this study. One building was located in the Sabzovot region of Tashkent, Uzbekistan, and was estimated to be at least 60 years old. The second set of samples was collected from Sukok of the Tashkent Region. In both cases, the samples were bored out from the walls as presented in Figure 3.

Figure 3. Sample collection.

The hole in the wall after taking the bored cylinder out is presented in Figure 4.

Figure 4. Adobe wall after specimen collection

Since the specimens could break inside the bore during the boring process, their length varied from specimen to specimen, as shown in Figure 5. For consistency, only long specimens were used in the study, and the short ones were discarded. The long specimens were cut to a shorter length to maintain a similar length-to-diameter ratio.

DOI: 10.3217/978-3-99161-057-1-152

Figure 5. Collected specimens before cutting them to the same length and selecting the best ones

The length and the diameter of each specimen are summarized in Table 1.

Table 1. Overall dimensions of adobe cylinders.

No	Length, mm	Diameter, mm	Geo-location
1	102	33	Sabzabot
2	110	52	Sabzabot
3	96	52	Sabzabot
4	105	52	Sabzabot
5	103	42	Sukok
6	104	44	Sukok
7	103	44	Sukok
8	103	43	Sukok

It is worth noting that the quality of the adobe material from these two geo-locations was noticeably different. The samples from Sabzovot were of a lighter color and were dense and uniform, whereas the samples from Sukok were of a darker color and had a few large voids, as shown in Figure 6. This difference played a significant role in the overall strength of the collected test specimens.

Figure 6. Adobe wall after specimen collection

3.2 Density results

The weight of each specimen was measured, and based on the calculated volume, the density was estimated as summarized in Table 2.

Table 2. Summary of density estimates.

No	Weight, g	Density, kg/m^3	Average
1	148.4	1701.0	1541.0
2	343.4	1470.0	
3	303.6	1489.1	
4	335.3	1503.7	
5	218.9	1534.0	1468.5
6	219.3	1386.8	
7	217.8	1390.7	
8	233.7	1562.4	

As presented in the table above, the average density of specimens from Sabzovot was slightly greater than that of the specimens from Sukok.

3.3 Compression test: specimen preparation

As mentioned earlier, the specimens varied in length. All of them were cut to maintain the same length-to-diameter ratio. Since the specimens were quite brittle, they were cut in a special device, as shown in Figure 7.

Figure 7. Adobe specimen in a cutting device

To distribute the forces at the ends of the samples, the adobe specimens were sulfur-capped for the compression test as presented in Figure 8.

Figure 8. Adobe specimens with sulfur caps

Finally, the adobe specimens were instrumented by bi-axial strain gages as presented in Figure 9. The legs of the gage were

DOI: 10.3217/978-3-99161-057-1-152

aligned with the longitudinal direction and the circumferential direction, respectively. A 40-mm long strain gage was used in this study.

Figure 9. Adobe specimen with bi-axial strain gage.

3.4 Compression test: strength

To measure the Young's modulus, Poisson's ratio, and strength of the specimens, they were tested using a compression test machine, as shown in Figure 10.

Figure 10. Adobe specimen in the compression test machine.

The compression load was applied at a constant rate of 25 N/s. A plot for Specimen No. 3 from the Sabzobot's geo-location showing the change of stress over time is presented in Figure 11.

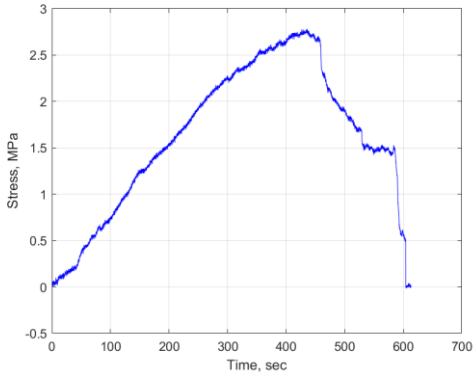

Figure 11. Force vs. time plot for Specimen No. 3.

As shown in the plot above, the stress steadily increases to the peak value, and there is a sharp decline in the compression stress capacity right after the peak value. A similar result was obtained for Specimen No. 4, as depicted in Figure 12. The peak load values were very close to each other, as summarized in Table 3. The table also shows the air humidity for each specimen on the day of testing.

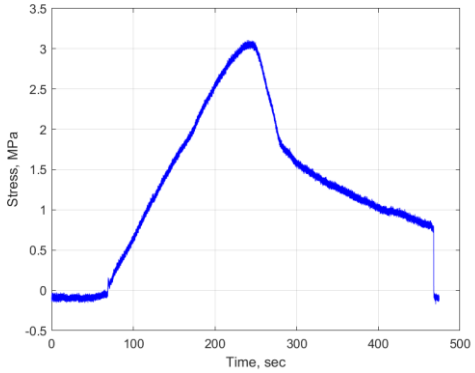

Figure 12. Stress vs. time plot for Specimen No. 4.

Table 3. Summary of compression strength (Sabzovot).

No	Peak load, N	Peak stress, MPa	Humidity, %
3	5911	2.78	30.0
4	6605	3.11	32.0

The results for the Sukok geo-location revealed different results. The strength capacity of the two tested specimens varied significantly, as presented in Figure 13 and Figure 14. The results are summarized in Table 4.

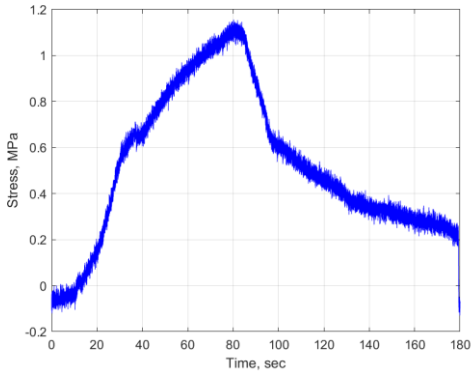

Figure 13. Stress vs. time plot for Specimen No. 6.

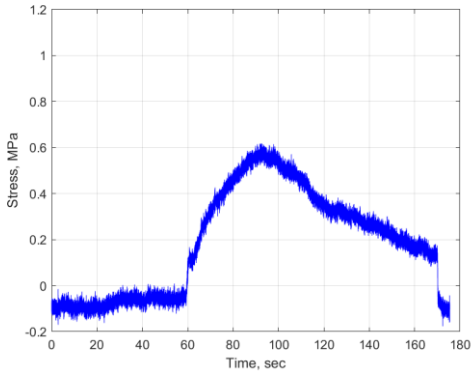

Figure 14. Stress vs. time plot for Specimen No. 7.

DOI: 10.3217/978-3-99161-057-1-152

Table 4. Summary of compression strength (Sukok).

No	Peak load, N	Peak stress, MPa	Humidity, %
6	2456	1.16	32.0
7	1312	0.62	32.0

The larger variability in the test results was expected because the Sabzobot samples were more homogeneous than the Sukok samples, which had a few relatively large voids.

3.5 Compression test: Young modulus

Several approaches to measuring Young's modulus in compression for cylinder-shaped specimens have been previously proposed and utilized [6-8]. One of the primary objectives of this paper was to utilize existing methods and select the most suitable one for achieving consistency in data reduction; therefore, the following all three approaches were employed and evaluated. First, a slope of a secant line between the start and end of the linear portion of the stress-strain curve was used to estimate Young's modulus [6]. In this paper, the modulus based on this approach is denoted by E_{LR}. Second, the Young's modulus calculation was based on the slope of a secant line between 5 and 50% of the peak stress [8]. $E_{05\text{-}50}$ denotes the modulus based on this approach. Third, a slope of the secant between 33.3 and 66.6% of the peak stress was used for estimating Young's modulus [7]. $E_{33\text{-}66}$ denotes the modulus based on this approach. All three procedures were employed in this paper, and their results were compared to one another.

As mentioned earlier, a bis-axial strain gage was installed on each test sample. The longitudinal leg of the strain gauge was used to estimate Young's modulus. A plot showing stress (σ) versus longitudinal stress (ε) for Specimen No. 3 is presented in Figure 15. The plot also displays the result of the linear regression, which was generated during the testing period, starting from loading and ending when the strain gage came out of the test specimen due to the gage's failure. It is worth noting that the latter point was very close to that when the peak stress occurs. The Young's modulus obtained from the linear regression (E_{LR}) is also presented in the same plot. It is worth noting that the R-squared value of the linear regression is close to unity, indicating a good fit. It can also be observed visually that the stress-strain curve can be closely approximated with a straight line. To reduce the noise of the recorded data, which can be visually observed in Figure 14 and Figure 14, a running average over seven points was used to filter out the noise for the Young's modulus calculations.

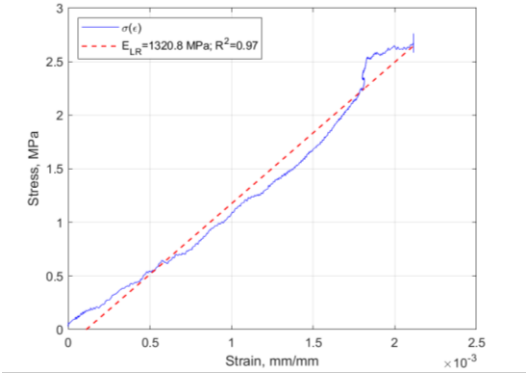

Figure 15. Stress vs. longitudinal strain plot for Specimen No. 3: Young's modulus from linear regression.

The results of the two other above-mentioned approaches for estimating Young's modulus are presented in Figure 16.

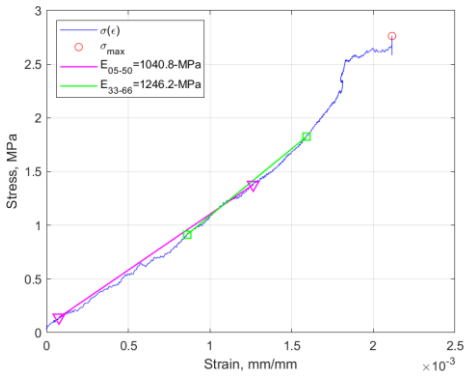

Figure 16. Stress vs. longitudinal strain plot for Specimen No. 3: two estimates of Young's modulus.

Similar results for Specimen No. 4 are presented in Figure 17 and Figure 18. As can be observed from the plots, the moment when the strain gage stopped working is very close to the moment when the maximum stress occurred.

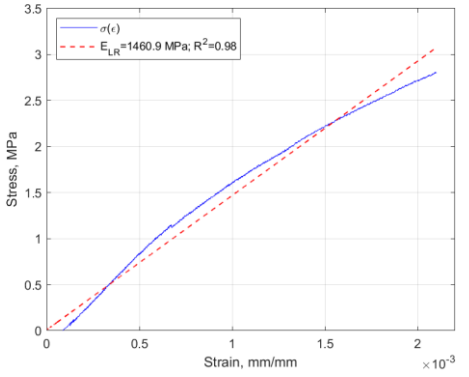

Figure 17. Stress vs. longitudinal strain plot for Specimen No. 4: Young's modulus from linear regression.

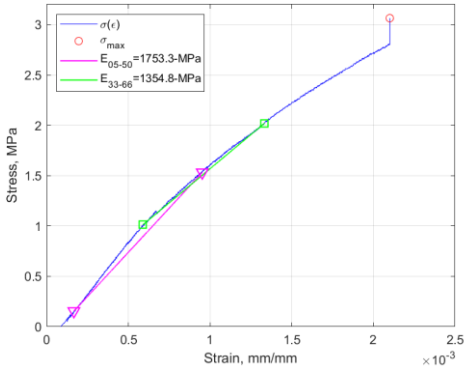

Figure 18. Stress vs. longitudinal strain plot for Specimen No. 4: two estimates of Young's modulus.

The results for the set collected from the Sabzobot geo-location show relatively large variation in the estimation of the Young's modulus, as summarized in Table 5. The variability of $E_{05\text{-}50}$ is significantly greater than that of the other two modules. It depends on the overall trend of the stress-strain curve: $E_{05\text{-}50}$ is less than $E_{33\text{-}66}$ when the curve opens upwards (concave up), and $E_{05\text{-}50}$ is greater than $E_{33\text{-}66}$ when it opens downwards

DOI: 10.3217/978-3-99161-057-1-152

(concave down). It is worth noting that the results for $E_{33\text{-}66}$ in both cases are closer to those for E_{LR}, although slightly lower.

Table 5. Summary of estimations of Young's modulus (Sabzovot).

No	E_{LR}, MPa (R^2)	$E_{05\text{-}50}$, MPa	$E_{33\text{-}66}$, MPa
3	1320.8 (0.97)	1040.8	1246.2
4	1460.9 (0.98)	1753.3	1354.8

The same calculation approaches were used for the sample set from the Sukok geo-location, and the results are summarized in Table 6. The stress-strain curves for Specimen 6, along with the respective values of Young's modulus, are presented in Figure 19 and Figure 20. It is worth noting that Specimen 7 data was very inconsistent with all other test results, and as such, it was considered an outlier.

Table 6. Summary of estimations of Young's modulus (Sukok).

No	E_{LR}, MPa (R^2)	$E_{05\text{-}50}$, MPa	$E_{33\text{-}66}$, MPa
6	1258.5 (0.99)	1198.9	1361.6
7	671.9 (0.95)	547.3	1003.8

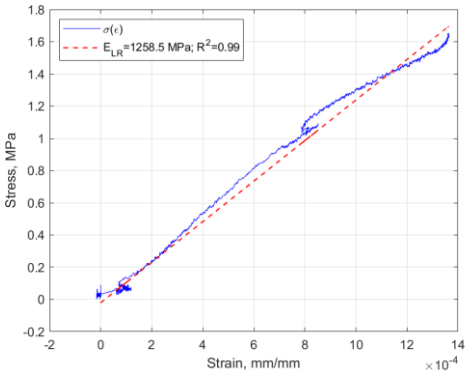

Figure 19. Stress vs. longitudinal strain plot for Specimen No. 6: Young's modulus from linear regression.

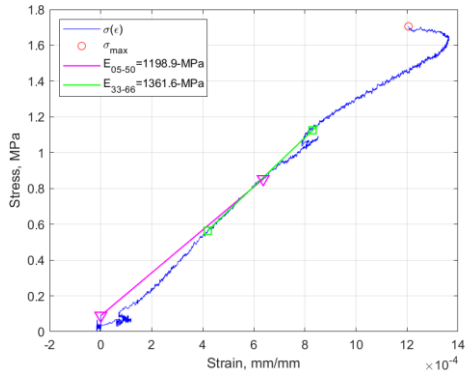

Figure 20. Stress vs. longitudinal strain plot for Specimen No. 6: two estimates of Young's modulus.

3.6 Compression test: Poisson's ratio

While the results for Young's modulus were reported for many locations worldwide [5], very limited information is available for the estimates of Poisson's ratio. This is especially true for the region of Central Asia. Therefore, one of the primary objectives of this paper was to address this issue and to have a complete set of mechanical properties of some adobe buildings. For this purpose, a strain gage was installed to read the circumferential strain (ʊ) of the adobe cylinders.

Poisson's ratio (ν) was obtained by using the following expression:

$$\nu = -\text{ʊ}/\varepsilon \tag{1}$$

The results for Specimen No. 3 are presented in Figure 21. In this plot, only a portion of the data was used to ensure that both longitudinal and circumferential strain gages yield reasonable data. The portion of the plot in red corresponds to the data when the stress was between 33.3% and 66.6% of the maximum stress. The plot shows that the general trend of the change of Poisson's ratio with stress is very close to linear. In the red portion of the data, the values vary from 0.12 to 0.16 with an average of 0.14.

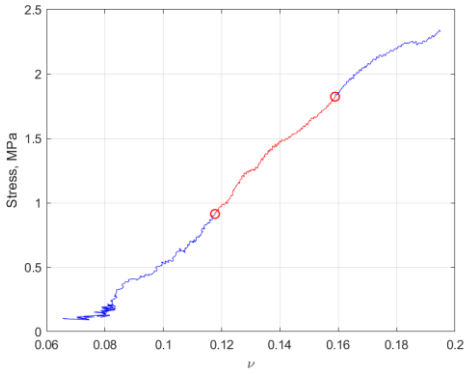

Figure 21. Stress vs. Poisson's ratio (ν) plot for Specimen No. 3: Sabzovot.

The respective results for Specimen No. 4 are shown in Figure 22. The plot shows that the general trend of the change of Poisson's ratio with stress is nonlinear. In the red portion of the data, the values vary from 0.12 to 0.18 with an average of 0.16.

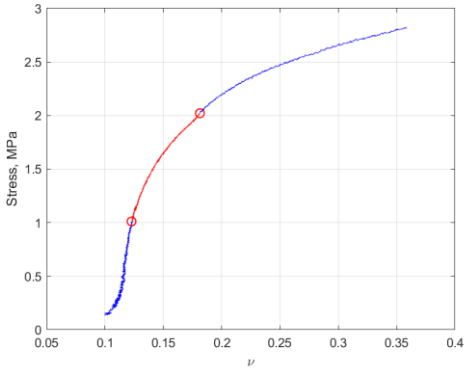

Figure 22. Stress vs. Poisson's ratio (ν) plot for Specimen No. 4: Sabzovot.

The test results for the specimens collected from Sukok geo-location are presented in Figure 23 and Figure 24. Specimen No. 6 (see Figure 23) yields stable results in the red portion of the data, where the value changes from 0.22 to 0.24 with an average of 0.23.

Specimen No. 7 was considered an outlier, and the results shown in Figure 24 serve as further evidence of this conclusion.

DOI: 10.3217/978-3-99161-057-1-152

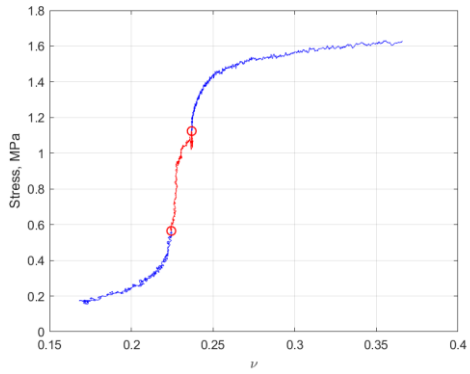

Figure 23. Stress vs. Poisson's ratio (ν) plot for Specimen No. 6: Sukok.

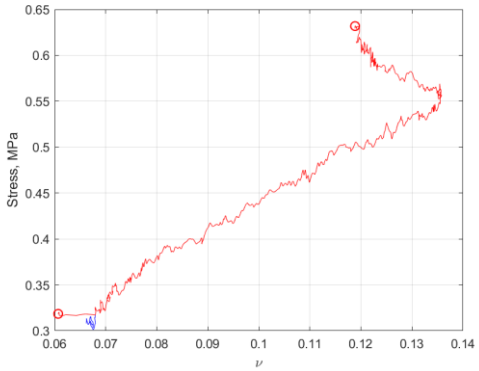

Figure 24. Stress vs. Poisson's ratio (ν) plot for Specimen No. 7: Sukok.

4 DISCUSSION AND CONCLUSIONS

The results discussed in the paper show that the testing of adobe specimens can be challenging. It greatly depends on the procedures followed during specimen collection, handling from the collection site to the test site, and preparation for the test. In addition, it depends on the overall quality of the adobe wall from which the specimens are collected. The quality of the adobe wall is controlled by following parameters: the quality of earth material available at the construction site, the curing time of the clay before forming it into a wall or a brick, the way the clay was placed into the walls, bonding aggregates added to the earth material (if any), the quality of the craftsmanship work, the curing process after forming the wall, and many others.

Several cylinder-shaped samples were collected from two geo-locations in Uzbekistan. The density of all specimens was determined before the tests. Since some of the collected samples did not have a uniform and homogeneous structure, a total of eight samples (out of eleven total) were used in the density estimation. The compression tests were performed on four of them to estimate the following mechanical parameters: compression strength, Young's modulus, and Poisson's ratio. Based on previous studies, three approaches for calculating Young's modulus were employed. The correlation between the previously published results (only corresponding to cylinder-shaped specimens from the literature) and the results obtained in this study was as follows.

The comparison of the results of this paper to the previously published results on compressive strength of cylindrical specimens is presented in Figure 25. As shown in the plot, the samples from Sabzobot geo-location were the greatest of all.

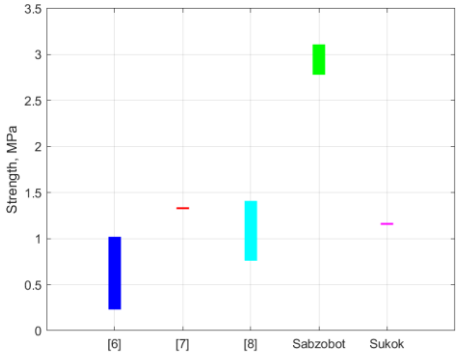

Figure 25. Compression strength results for Sabzovot and Sukok geo-locations compared to previously published [6], [7], and [8].

When comparing the Sabzovot and Sukok sets to [6], the compression strength of the adobe samples was slightly greater: the lowest value (excluding the outlier) is 1.16 MPa, versus 1.02 MPa [6]. Young's modulus was significantly lower: 1,461 MPa is the largest value obtained in this work, excluding the outlier, compared to 7,609 MPa reported earlier [6]. When compared to [7], the compression strength of adobe samples was slightly lower: the lowest value (excluding the outlier) is 1.16 MPa versus 1.33 MPa [7]. Young's modulus obtained in this study was significantly greater: 1,461 MPa is the largest value (excluding the outlier) versus 802 MPa reported earlier [7]. When compared to [8], the compression strength of adobe samples was slightly lower: the lowest value (excluding the outlier) is 1.16 MPa versus 1.71 MPa [7]. Young's modulus obtained in this study was significantly greater: 1,461 MPa was the largest value (excluding the outlier) versus 92 MPa published earlier [8].

The study showed that $E_{05\text{-}50}$ depends on the direction of the overall curvature of the stress-strain curve and, as such, can have much larger variation. At the same time, E_{LR} and $E_{33\text{-}66}$ yielded more similar results.

No literature references were found with respect to the experimental estimation of Poisson's ratio for adobe cylinders. The results of this study showed that Poisson's ratio is most likely stress-dependent, and for stress between 33.3% and 66.6% of the maximum stress, it can vary from about 0.12 to 0.24.

The results of this study will be used in finite element modelling of Chadra Hauly (Khorezm Region, Uzbekistan). The finite element mesh of the monument was generated by a laser scanner [3]; only the mechanical parameters of adobe were missing to generate a realistic model. This study fulfilled this need. The team is working on collecting more samples from other geo-locations to develop an extensive database of pakhsa properties in Central Asia.

It is worth noting that only a few test results are discussed here as representative examples. The research group is working on collecting more samples from other adobe buildings, including heritage buildings.

DOI: 10.3217/978-3-99161-057-1-152

ACKNOWLEDGMENTS

The authors would like to acknowledge the partial financial support and technical assistance of the Department of Civil and Environmental Engineering at the University of California, Berkeley.

REFERENCES

[1] Takhirov S., Rakhmonov B.S., Nafasov R., Samandarov A., Sultanova S., Akhmedov M.M., Shamansurov R.A. (2024). First Step Toward Preservation of Ancient Toprak Qala in Uzbekistan: Estimation of Erosion and Deterioration Rates by Laser Scanning. RILEM Bookseries, 47, pp. 581 - 590, Book chapter. DOI: 10.1007/978-3-031-39603-8_47. https://www.scopus.com/inward/record.uri?eid=2-s2.0-85170362061&doi=10.1007%2f978-3-031-39603-8_47&partnerID=40&md5=5d04041ade6b40f3983a6b064a8d5f78.

[2] Frachetti, M.D., Berner, J., Liu, X. et al. Large-scale medieval urbanism traced by UAV–lidar in highland Central Asia. Nature 634, 1118–1124 (2024). https://doi.org/10.1038/s41586-024-08086-5.

[3] Takhirov S, Rakhmonov B, Akhmedov M, and Blondet M (2024) Structural Health Monitoring of Chadra Hauly (Khorezm, Uzbekistan) by Means of Laser Scanning. International Conference: Ensuring seismic safety and seismic stability of buildings and structures, applied problems of mechanics, Tashkent, Uzbekistan, May 27-29, 2024.

[4] ADB (2025). Tajikistan: Case Study Report on Resilient Community Housing. Consultant's report (TA 6929-REG).

[5] Silveira D et al. (2021). Mechanical Characterization of Adobe Bricks. In: Varum, H., Parisi, F., Tarque, N., & Silveira, D. (Eds.), Structural Characterization and Seismic Retrofitting of Adobe Constructions. Building Pathology and Rehabilitation, vol 20. Springer, Cham. https://doi.org/10.1007/978-3-030-74737-4_3.

[6] Silveira D, Varum H, Costa A (2013) Influence of the testing procedures in the mechanical characterization of adobe bricks, Construction and Building Materials, Volume 40, Pages 719-728, ISSN 0950-0618,https://doi.org/10.1016/j.conbuildmat.2012.11.058.

[7] Rodríguez-Mariscal JD, Solís M, Cifuentes H (2018) Methodological issues for the mechanical characterization of unfired earth bricks. Constr Build Mater 175: 804–814.

[8] Illampas R, Ioannou I, Charmpis DC (2014) Adobe bricks under compression: experimental investigation and derivation of stress-strain equation. Constr Build Mater 53: 83–90.

[9] ASTM (2023) ASTM C67/C67M-21: Standard Test Methods for Sampling and Testing Brick and Structural Clay Tile.